WATER RESOURCES RESEARCH, VOL. 30, NO. 4, PAGES 903–912, APRIL 1994

A vertical equilibrium model for assessing nonaqueous phase liquid contamination and remediation of groundwater systems

Yu-Shu Wu, P. S. Huyakorn, and N. S. Park
HydroGeoLogic, Incorporated, Herndon, Virginia

Abstract. A numerical model has been developed to provide areal analyses of the three-dimensional spreading of immiscible liquids in groundwater systems. The model is intended for specific use in prediction of hydrocarbon spreading from subsurface leaks and spills and in design and performance evaluation of remedial schemes. The mathematical formulation is based on vertical integration of the three-dimensional two-phase flow equations and incorporation of the concept of gravity-capillary vertical equilibrium (GCVE) in which a vertical balance of gravitational and capillary forces is assumed. History-dependent pseudo functions of capillary pressure and relative permeabilities are introduced for the present GCVE model. A direct numerical procedure for evaluating the pseudo functions is derived and verified using an example given in the petroleum literature. An overview of numerical techniques for solving the nonlinear governing equations is presented. Special schemes for handling production wells are derived. Simulation examples are provided to verify, validate, and demonstrate utility of the model. Numerical results obtained from the GCVE model are compared with analytical and rigorous multiphase three-dimensional numerical solutions. The model is further validated using data from a laboratory investigation on waterflood, five-spot well performance. The results of these comparisons show the validity of the GCVE modeling assumptions and accuracy and robustness of the proposed formulations and computational schemes. The numerical study also indicates that the present model is highly efficient and suitable for field simulations on personal computers or workstations.

Introduction

The release and subsurface migration of nonaqueous phase liquids (NAPL) such as oily wastes, petroleum products, and industrial chemicals have caused serious groundwater contamination problems throughout the United States. Modeling assessments of contaminant migration and remedial options are becoming crucial due to the increased necessity to address and mitigate the environmental problems. A number of numerical models have been documented which describe the simultaneous flow of groundwater and NAPL in unconfined aquifer systems. However, most field-scale simulations performed to date have been limited to cross-sectional analyses involving a vertical slice through unsaturated and/or saturated zones [*Abriola and Pinder*, 1985; *Faust*, 1985; *Forsyth*, 1988, 1991; *Kaluarachchi and Parker*, 1989]. Such two-dimensional models do not provide adequate treatment of many field situations which involve areal variations of aquifer properties and/or dominant horizontal transverse flow components due to, for example, implementation of remedial schemes. Three-dimensional multiphase flow models have been described recently by *Faust et al.* [1989], *Letniowski and Forsyth* [1991], and *Huyakorn et al.* [1992a, b]. However, the computational burden of fully three dimensional analyses still imposes severe constraints on their field application.

An alternative simulation approach to complex field problems is via the use of an areal model based on vertical integration of the three-dimensional multiphase flow equations under a vertical equilibrium (VE) or hydrostatic assumption for each phase. Such an approach is widely known in the petroleum reservoir modeling literature and is based on the original works of *Coats et al.* [1967, 1971] and *Martin* [1968]. The VE modeling approach offers several advantages which include reducing the spatial dimensionality and nonlinearity of the problem. Thus savings in computational resources can be substantial.

Several VE numerical models have been proposed for areal simulation of NAPL migration [*Hochmuth and Sunada*, 1985; *Kaluarachchi et al.*, 1990; *Parker et al.*, 1990, 1992]. However, these models are applicable only to light nonaqueous phase liquids (LNAPL). Furthermore, there are some other shortcomings in the model formulations. The model presented by *Hochmuth and Sunada* [1985] is based on sharp-interface formulations that incorporate residual saturations only in the storage terms of the equations. However, the effects of residual saturations on the storage terms vanish when steady state conditions are reached under pulse NAPL source conditions. Therefore situations where the NAPL mass becomes immobile cannot be predicted. The model presented by *Kaluarachchi et al.* [1990] uses a more sophisticated formulation that accounts for the effects of capillary pressure on saturation distribution. However, their model suffers some drawbacks due to the limitation of the assumptions used [see *Parker and Lenhard*, 1989]. For the VE condition is assumed not only in the liquid-saturated

0043-1397/94/93WR-03412$05.00

zones but also in the overlying vadose zone. Physically, vertical equilibrium implies uniform vertical distributions of water and NAPL potentials. In the vadose zone, however, the vertical gradients of the fluid potentials are usually significant because of the impact of infiltration and the tendency of the NAPL to move downward toward the water table. Consequently, the VE assumption (which is essentially similar to the Dupuit-Forchheimer assumption in groundwater hydrology) may be violated in the unsaturated zone.

The present mathematical formulation and numerical model differ from the works of *Parker and Lenhard* [1989] and *Kaluarachchi et al.* [1990] in the following respects. First, we apply the VE assumption, which corresponds to the Dupuit-Forchheimer assumption in groundwater hydrology, only in the liquid-saturated zone. Unlike the previous formulation, the domain of vertical integration used in the present formulation does not include the vadose zone. Second, the present model incorporates residual NAPL saturation via the use of history-dependent pseudo functions evaluated using a rigorous numerical integration procedure that accommodates any type of rock of soil (real) capillary pressure and relative permeability data. In the previous work of *Parker and Lenhard* [1989] an analytical integration procedure was used to evaluate the pseudo functions. The procedure assumes zero residual NAPL saturation and limits the choice of real capillary pressure curve to the Brooks-Corey closed-form expression. Third, the governing equations are handled in our model using rigorous, mass-conservative numerical approximation and Newton-Raphson nonlinear solution schemes with optimal choice of primary dependent variables. Finally, we include in our gravity-capillary vertical equilibrium (GCVE) numerical model a rigorous, fully implicit scheme for treating production wells. The well boundary conditions considered by our model are more practical than those assumed by the previous model.

Robust and efficient numerical techniques have been incorporated and verified in our proposed model to enable practical simulations of site-specific field problems on personal computers and workstations. The governing equations are discretized using a modified Galerkin finite element method with an influence coefficient scheme for element matrix computation, thereby avoiding numerical integration. Nonlinearities are treated using the Newton-Raphson technique. The convergence and efficiency of the overall nonlinear solution procedure are enhanced by an advanced time-stepping control scheme which takes the full advantage of the Newton-Raphson scheme.

GCVE Mathematical Model and Assumptions

The GCVE formulation assumes that vertical equilibrium occurs in the aquifer as a result of a gravity-capillary balance. The model thus takes into account the existence of a capillary transition zone in which there is a gradual variation of NAPL saturation. For a two-phase (water-NAPL) system the mathematical conditions for GCVE may be expressed as [*Coats et al.*, 1967]

$$\frac{\partial \Phi_w}{\partial z} = \frac{\partial \Phi_n}{\partial z} = 0 \tag{1}$$

$$p_c(x, y, z) = p_c^*(x, y) + (\rho_w - \rho_n) g (z - z^*) \tag{2}$$

where Φ_w and Φ_n are water and NAPL potentials, respectively, x and y are areal coordinates, z is the upward vertical coordinate, ρ_w and ρ_n are water and NAPL densities, g is the gravitational constant, $p_c^*(x, y)$ is a capillary pressure taken at an areal point on a reference surface located at z^*, and $p_c(x, y, z)$ is the capillary pressure at any other point along the vertical line passing through (x, y) and within the three-dimensional groundwater system.

Equations (1) and (2) simply indicate that under the state of GCVE the vertical gradients of fluid potentials are zero and that the knowledge of capillary pressure at any point on the reference surface establishes the variation of capillary pressure along the vertical line through that point. For convenience we let the reference surface coincide with the top liquid table when dealing with an unconfined system and the top of the aquifer when dealing with a confined system. Equation (2) thus becomes

$$p_c(x, y, z) = \bar{p}_c(x, y) - (\rho_w - \rho_n) g (Z_T - z) \tag{3}$$

where Z_T is the elevation of the top liquid table, and $\bar{p}_c$ now corresponds to $z^* = Z_T$.

The governing equations of the GCVE model can be derived by performing vertical integration of three-dimensional two-phase flow equations from the aquifer base Z_B to the top surface Z_T. The resulting equations may be written in the form

$$\frac{\partial}{\partial x}\left[\bar{k}_x \tau_{lx} \frac{\partial \Phi_l}{\partial x}\right] + \frac{\partial}{\partial y}\left[\bar{k}_y \tau_{ly} \frac{\partial \Phi_l}{\partial y}\right] = \frac{\partial}{\partial t}(b \rho_l \bar{\phi} \bar{S}_l) - \dot{M}_l \tag{4}$$

$$l = w, n$$

$$\bar{k}_i = \frac{1}{b}\int_{Z_B}^{Z_T} k_i(z)\, dz \qquad i = x, y \tag{5a}$$

$$\tau_{li} = b \bar{k}_{rli} \rho_l / \mu_l \qquad i = x, y \tag{5b}$$

$$\bar{k}_{rli} = \frac{\int_{Z_B}^{Z_T} k_i(z) k_{rl}(z)\, dz}{\int_{Z_B}^{Z_T} k_i(z)\, dz} \qquad i = x, y \tag{5c}$$

$$\bar{\phi} = \frac{1}{b}\int_{Z_B}^{Z_T} \phi(z)\, dz \tag{5d}$$

$$\bar{S}_l = \frac{\int_{Z_B}^{Z_T} \phi(z) S_l(z)\, dz}{\int_{Z_B}^{Z_T} \phi(z)\, dz} \tag{5e}$$

Note that k_i is the intrinsic permeability, k_{rl} is the relative permeability of phase l, b is the liquid-saturated thickness ($b = Z_T - Z_B$), ϕ is the effective porosity, μ_l is the dynamic viscosity of phase l, the overbar denotes vertical averaging, and M_l is the net fluid mass flux term resulting from such factors as well pumping or injection, NAPL

Equation (4) is supplemented by the following relations:

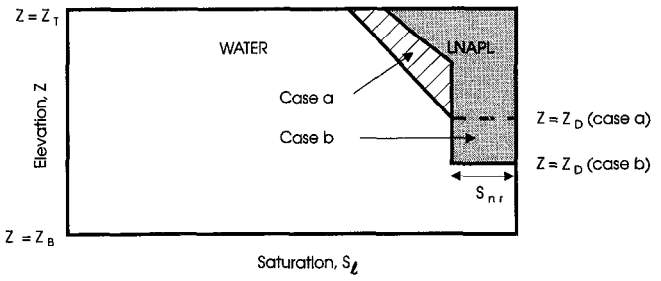

Figure 1. Vertical profiles of saturation that produce the same value of $\bar{S}_n$ for two cases of (a) mobile LNAPL and (b) partly immobile LNAPL.

$$\bar{S}_w + \bar{S}_n = 1 \tag{6}$$

$$\Phi_n = \Phi_w + \bar{p}_c - g(\rho_w - \rho_n)Z_T \tag{7}$$

$$\bar{k}_{rl} = \bar{k}_{rl}(\bar{S}_w, Z_D) \tag{8}$$

$$\bar{p}_c = \bar{p}_c(\bar{S}_w, Z_D) \tag{9}$$

where $\bar{p}_c$ and $\bar{k}_{rl}$ are the pseudo capillary and relative permeability functions, respectively. In general, these functions are dependent on not only $\bar{S}_w$ (or $\bar{S}_n$) but also a second parameter Z_D that reflects the history of NAPL contamination, as will be shown in the next section. Note that we need the rock or soil capillary pressure and relative permeability curves to evaluate the pseudo functions in the GCVE model.

Evaluation of Pseudo Functions

History-Dependent Pseudo Functions

In order to obtain a realistic simulation of the NAPL contamination problem, it is essential to account for the fact that the flow domain may be partly free of NAPL, and application of a remedial scheme will eventually leave behind the residual (irreducible) NAPL saturation (S_{nr}) in the contaminated zone. Simply stated, one needs to keep track of the residual NAPL mass in the evaluation of pseudo relative permeabilities and pseudo capillary pressure.

An original numerical procedure for evaluating the pseudo functions of two-phase GCVE petroleum reservoir models was developed by *Coats et al.* [1967]. However, the standard procedure and its three-phase extension by *Martin* [1968] neglect history dependency of the pseudo functions. Note that in the simulation of reservoir performance it is common to assume that oil is omnipresent in the reservoir formation. In their original work, *Coats et al.* [1967] consider two-phase flow of oil and gas and regard the nonwetting (gas) phase as having zero residual saturation. Hence the issue of history dependency of the pseudo functions becomes irrelevant in such cases.

In the general context of NAPL contamination in a groundwater system the pseudo functions, $\bar{k}_{rl}$ and $\bar{p}_c$, depend not only on $\bar{S}_w$ or $\bar{S}_n$ but also on the history of saturation distribution. Consider the case of a LNAPL lens that is subject to remediation by well pumping. If the irreducible LNAPL mass is nonzero, there may exist two different vertical profiles of saturation that give the same of $\bar{S}_n$ as shown in Figure 1. Note that $\bar{S}_n$ is equal to the shaded area divided by $(Z_T - Z_B)$. Since $\bar{S}_n$ is the vertically averaged LNAPL saturation, its value is not unique unless the cut off (maximum penetration) depth corresponding to the elevation Z_D is specified. To ensure uniqueness of the numerical solution we define the pseudo functions as given by (8) and (9). In view of the fact that the LNAPL lens floats on the water table, we choose the reference surface to correspond to $z^* = Z_T$, which is the top of the liquid-saturated zone. For convenience in presenting our history-dependent scheme for pseudo function evaluation, it is assumed that the total liquid-saturated thickness $(Z_T - Z_B)$ is approximately constant with time. For each time step the computational procedure consists of three parts: (1) determining the pseudo capillary function $\bar{p}_c(\bar{S}_w, Z_D)$, (2) determining the pseudo relative permeability functions $\bar{k}_{rw}(\bar{S}_w, Z_D)$ and $\bar{k}_{rn}(\bar{S}_w, Z_D)$, and (3) updating the value of Z_D.

Pseudo Capillary Pressure

For each specified nodal point (x_I, y_I) of the areal grid adopted for the numerical solution we first determine (at the beginning of the current time step) whether the LNAPL is present or not. If $\bar{S}_n \leq 0$ (where $\bar{S}_n$ is the current iterate of the vertically averaged LNAPL saturation at the nodal point), there is no LNAPL, and $\bar{p}_c$ is simply set to zero. If $\bar{S}_n > 0$, the LNAPL is present, and the pseudo capillary pressure function $\bar{p}_c$ versus $\bar{S}_w$ needs to be evaluated via numerical integration over a selected number of intervals: $Z_B \leq z_i \leq Z_T$ $(i = 1, 2, \cdots, NZ + 1)$, where NZ is the number of depth intervals, and $Z_T = z_1 > z_2 > \cdots > Z_{NZ+1} = Z_B$. The computational procedure is described below.

1. From the soil or rock (real) capillary pressure curve (p_c versus S_w) supplied to the computer code, determine the minimum and maximum capillary pressure values, $p_{c\min}$ and $p_{c\max}$, and assume a series of $\bar{p}_c$ values such that

$$p_{c\min} \leq \bar{p}_{cj} \leq p_{c\max} \qquad j = 1, 2, \cdots, NC + 1 \tag{10}$$

where NC is the number of increments. For a particular $\bar{p}_{cj}$, calculate the vertical distribution $(Z_T - z_i)$ of the real capillary pressure using the relationship

$$p_{cj} = \bar{p}_{cj} - g(\rho_w - \rho_n)(Z_T - z_i) \tag{11}$$

and by varying i from 1 to $NZ + 1$.

2. Calculate the $S_{nj}(z_i)$ distribution using $p_{cj}(z_i)$ and input p_c data (real capillary pressure curve) subject to the following constraint:

$$S_{nj}(z_i) \geq S_{nr} \qquad \text{for } z_i \geq Z_D \tag{12a}$$

$$S_{nj}(z_i) \leq 1 - S_{wr} \qquad \text{for } z_i < Z_D \tag{12b}$$

where Z_D is the value of z coordinate that corresponds to the maximum depth of penetration of LNAPL up to the end of the previous time step, and S_{nr} and S_{wr} are the residual saturations of LNAPL and water, respectively.

3. Compute the vertically averaged water saturation from

$$\bar{S}_{wj} = 1 - \bar{S}_{nj} \tag{13}$$

where $\bar{S}_{nj}$ is the vertically averaged LNAPL saturation obtained in accordance with (5e), and by numerical integration of the profile of $S_w(z)$. For our modeling purposes the trapezoidal rule for numerical integration yields sufficient accuracy.

Note that repetition of steps 1–3 will give one pseudo capillary curve (i.e., $\bar{p}_{cj}$ versus $\bar{S}_{wj}$) for each specified value of Z_D. By varying the value of Z_D a family of $\bar{p}_c(\bar{S}_w)$ curves will be obtained. This completes the generation of the pseudo capillary pressure relations for the nodal points where LNAPL exists.

Pseudo Relative Permeabilities

For a specified nodal point of the selected areal grid, the pseudo relative permeabilities to water and LNAPL, $\bar{k}_{rw}$ and $\bar{k}_{rn}$, are determined by first checking whether there is LNAPL mass at the nodal point. If the LNAPL is absent ($\bar{S}_n \leq 0$), then $\bar{k}_{rw}$ and $\bar{k}_{rn}$ are simply set equal to 1 and 0, respectively. If the LNAPL is present ($\bar{S}_n > 0$), we need to determine if it is mobile or immobile. The condition of immobile LNAPL corresponds to $\bar{S}_n \leq (Z_T - Z_D)S_{nr}/b$. If this condition is satisfied, then $\bar{k}_{rn}$ is zero and $\bar{k}_{rw}$ is given by

$$\bar{k}_{rw} = \frac{1}{b}\left[(Z_D - Z_B) + k^*_{rw}(Z_T - Z_D)\right] \tag{14}$$

where k^*_{rw} is the relative permeability to water at the residual LNAPL saturation.

If the LNAPL is mobile ($\bar{S}_n > (Z_T - Z_B)S_{nr}/b$), the pseudo relative permeability values need to be evaluated via numerical integration over the selected number of depth intervals (NZ). The computational procedure is described below.

1. Use the current value of $\bar{S}_n$ to determine the corresponding value of $\bar{p}_c$ by interpolation of the $\bar{p}_c(\bar{S}_w)$ function determined for the specified grid point as described in the previous section. Knowing the $\bar{p}_c$ value at the reference surface, we can determine the vertical profile of the real capillary pressure from

$$p_c(z_i) = \bar{p}_c - (\rho_w - \rho_n)g(Z_T - z_i) \tag{15}$$

where i ranges from 1 to $NZ + 1$.

2. Use the $p_c(z_i)$ values to compute the vertical profile of LNAPL saturation $S_n(z_i)$ by interpolation of the real capillary pressure curve and application of the following constraints:

$$S_w + S_n = 1 \tag{16}$$

$$S_n(z_i) \geq S_{nr} \qquad \text{for } z_i \geq Z_D \tag{17a}$$

$$S_n(z_i) \leq 1 - S_{wr} \qquad \text{for } z_i < Z_D \tag{17b}$$

3. In order to conserve mass, the desired vertical profile of LNAPL must also satisfy one additional constraint:

$$\frac{1}{b}\int_{Z_c}^{Z_T} S_n(z_i)\, dz = \bar{S}_n \tag{18}$$

where Z_c is the cut off elevation below which $S_n(z_i)$ is set to zero or S_{nr}. Note that for the numerical solution to be acceptable, Z_c must be greater or equal to Z_B. The correct value of Z_c is readily determined by incremental evaluation of the integral from Z_T downward (scanning through z_i) until the cumulative value of the left-hand side of (18) exceeds the $\bar{S}_n$ value, say at $i = i^*$. We then use linear interpolation to obtain Z_c. Noting that $z_{i^*-1} < Z_c < z_{i^*}$, we move z_{i^*} to Z_c for convenience in evaluating the pseudo relative permeabilities.

4. Compute vertical distributions of k_{rn} and k_{rw} using $S_n(z_i)$ ($i = 1, 2, \cdots, i^*$), and the rock or soil relative permeability data, and then evaluate the pseudo relative permeabilities in accordance with (5c). If it is assumed that the intrinsic permeabilities (k_x and k_y) are vertically uniform, then $\bar{k}_{rn}$ and $\bar{k}_{rw}$ are given by

$$\bar{k}_{rn} = \frac{1}{b}\left[\int_{Z_c}^{Z_T} k_{rn}(z_i)\, dz\right] \tag{19}$$

$$\bar{k}_{rw} = \frac{1}{b}\left[\int_{Z_c}^{Z_T} k_{rw}(z_i)\, dz\right] + \Delta\bar{k}_{rw} \tag{20}$$

where

$$\begin{aligned} \Delta\bar{k}_{rw} &= (Z_c - Z_B)/b && \text{if } Z_c < Z_D \\ \Delta\bar{k}_{rw} &= (Z_c - Z_D)k^*_{rw}/b + (Z_D - Z_B)/b && \text{if } Z_c \geq Z_D \end{aligned} \tag{21}$$

Updating of Z_D Value

After the numerical solution has converged at the end of a time step, the values of Z_D at various grid points need to be updated. For each specified grid point we first check whether the converged value of vertically averaged saturation at the current time level, $\bar{S}_n^{k+1}$, satisfies the condition $\bar{S}_n^{k+1} \leq \bar{S}_{n\max}$, where $k + 1$ denotes the current time level, and $\bar{S}_{n\max}$ is the maximum vertically average LNAPL saturation attained thus far at the grid point (x_I, y_I). If this condition is satisfied, no updating of Z_D is necessary. Otherwise, the following procedure applies:

1. With the selected values of $z_i (i = 1, 2, \cdots, NZ + 1)$, compute the vertical distribution of capillary pressure using the equation

$$p_c^{k+1}(z_i) = \bar{p}_c^{k+1} - (\rho_w - \rho_n)g(Z_T - z_i) \tag{22}$$

where $\bar{p}_c^{k+1}$ is the pseudo capillary pressure corresponding to $\bar{S}_n^{k+1}$.

2. Use the $p_c^{k+1}(z_i)$ values determined from step 1 to compute $S_n^{k+1}(z_i)$ by interpolation of the input p_c versus S_w data and application of the following constraints:

$$S_w^{k+1} + S_n^{k+1} = 1 \tag{23}$$

$$S_n^{k+1}(z_i) \geq S_{nr} \qquad \text{for } z_i \geq Z_D^k \tag{24}$$

$$S_n^{k+1} \leq 1 - S_{wr} \qquad \text{for } z_i < Z_D^k \tag{25}$$

where Z_D^k is the elevation corresponding to the maximum LNAPL penetration depth up to the end of the previous time step.

3. Determine the current Z_D value Z_D^{k+1} using

$$\frac{1}{b}\int_{Z_D^{k+1}}^{Z_T} S_n^{k+1}(z_i)\, dz = \bar{S}_n^{k+1} \tag{26}$$

with the constraint $Z_D^{k+1} \leq Z_D^k$.

Verification of Pseudo Function Computational Scheme

In order to verify the proposed scheme for evaluating the pseudo functions we use one of the petroleum reservoir examples given by *Willhite* [1986]. A homogeneous and isotropic reservoir of constant thickness, $b = 40$ ft (12 m), is considered. The LNAPL of concern is light oil with a density

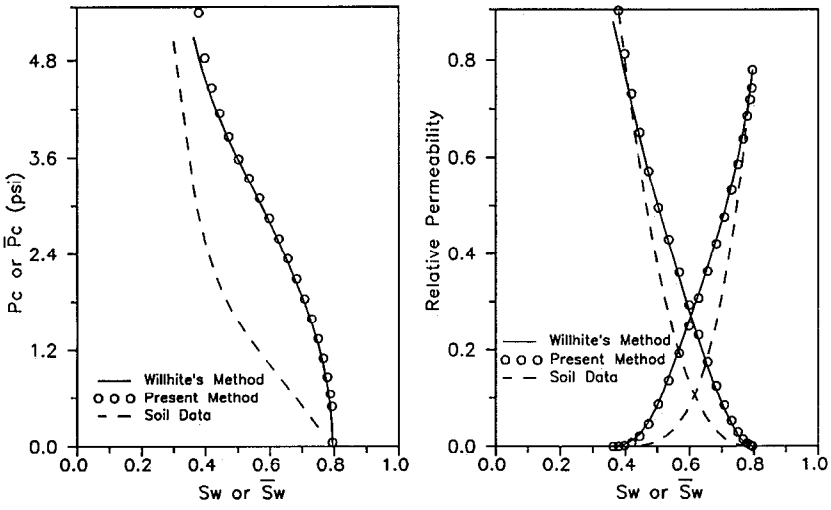

Figure 2. Verification of the pseudo function computational scheme by comparison with simulated curves provided by *Willhite* [1986, p. 151].

of 49.92 lb ft^{-3} (799.6 kg m^{-3}). The base of the reservoir is horizontal at $Z_B = 0$, and the LNAPL is assumed to be ubiquitous (i.e. Z_D is set equal to zero to correspond to the maximum LNAPL penetration thickness of 40 ft (12 m)). The physical parameter values and relative permeability and capillary pressure data required are from *Willhite* [1986]. The rock and pseudo functions are plotted in Figure 2. It can be seen that our calculated values of the pseudo functions are in excellent agreement with the corresponding curves obtained by *Willhite* [1986] using a trial and error scheme. Note that his trial and error scheme begins to deteriorate toward the asymptotic part of the pseudo capillary curve, whereas our direct scheme still works fairly well. More significant is the relative permeability curve, which shows exact agreement between soil data and the results from the current scheme near $S_w = S_{wr}$. Willhite's method failed to give these points.

Numerical Solution Schemes and Model Output

Numerical Scheme

The model formulation employs an areal finite element grid to represent the liquid-saturated zone of the aquifer domain. The governing equations represented by (4) are approximated using the Galerkin procedure with upstream weighting of phase mobilities and storage matrix lumping. Time integration is performed using a fully implicit finite difference scheme. This leads to the following system of algebraic equations:

$$R_I^l(\Phi_{II}, \bar{S}_{II}) \equiv \sum_{J \in \eta_1} \tau_{IIJ}^{ll} \gamma_{IJ} (\Phi_{II} - \Phi_{IJ})^{t+\Delta t} + \frac{B_{II}}{\Delta t} [(b\bar{\phi}\rho_l \bar{S}_l)_I^{t+\Delta t} - (b\bar{\phi}\rho_l \bar{S}_l)_I^t] - \dot{M}_{II} = 0 \quad (27)$$

$$l = w, n \qquad I = 1, 2, \cdots, n$$

where I and J are nodal indices ranging from 1 to n with n being the number of nodes in the grid, superscript $t + \Delta t$ denotes the current time, Δt is the time increment, $\dot{M}_{II}$ is the nodes, τ_{IIJ}^{ll} is the upstream weighted value of the l phase mobility for the discrete flow between nodes I and J, γ_{IJ} is the transmissivity coefficient for the flow between nodes I and J, and B_{II} is the storage matrix elements.

The nonlinearity of the discretized equations is handled using a residual-based Newton-Raphson iterative procedure with the LNAPL potential (Φ_n) and vertically averaged saturation ($\bar{S}_w$) chosen as the primary variables. Application of the Newton-Raphson procedure to the above equations yields

$$\frac{\partial R_I^n}{\partial \Phi_{nJ}} \Delta\Phi_{nJ} + \frac{\partial R_I^n}{\partial \bar{S}_{wJ}} \Delta\bar{S}_{wJ} = -(R_I^n)^k \quad (28a)$$

$$\frac{\partial R_I^w}{\partial \Phi_{nJ}} \Delta\Phi_{nJ} + \frac{\partial R_I^w}{\partial \bar{S}_{wJ}} \Delta\bar{S}_{wJ} = -(R_I^w)^k \quad (28b)$$

where

$$\Delta\Phi_{nJ} = \Phi_{nJ}^{k+1} - \Phi_{nJ}^k \quad (29a)$$

$$\Delta\bar{S}_{wJ} = \bar{S}_{wJ}^{k+1} - \bar{S}_{wJ}^k \quad (29b)$$

and k and $k + 1$ denote previous and current iteration levels, respectively.

During each iteration the linearized system of algebraic equations is solved for the nodal unknowns using a direct banded block matrix solver. The nodal values of the primary variables are then updated for the next iteration. If necessary, time step adjustments are made to handle a convergence problem and obtain an efficient transient simulation. The updating of the nodal values of the unknown variables is performed using a scheme with an underrelaxation factor determined automatically and dependent upon the maximum convergence errors for the entire grid.

Incorporation of Initial and Boundary Conditions

The initial conditions required to start a transient simulation are introduced by specifying the values of the primary variables (Φ_n, $\bar{S}_w$) at all nodes. These initial values may be system. In some instances the initial conditions for a current

simulation correspond to the final results of a previous simulation.

Boundary conditions for the multiphase flow equations may be specified in terms of nodal values of fluid potentials and mass fluxes. Prescribed flux conditions are treated simply by adding the specified nodal flux values to the right-hand side of the corresponding nodal equations. In practice, the flux terms of interest may include lateral fluxes due to ambient groundwater flow as well as vertical fluxes resulting from such mechanisms as groundwater recharge at the water table and leakage through aquitards, NAPL input due to leakage, spills, or subsurface disposal, and withdrawal of NAPL and water by wells, galleries, or drains.

Prescribed potential conditions of $\Phi_{lI} = \bar{\Phi}$ are incorporated in the matrix system using a source/sink term fully implicitly, as treated in multiphase flow simulations [*Forsyth*, 1988].

Treatment of Wells

For the situation involving a well pumping at a prescribed volumetric rate of total liquid production Q_L the well is represented by a single node (say node I) in the selected areal grid. The total volumetric liquid flux at the node is the sum of LNAPL and water fluxes. Thus

$$Q_L = Q_{wI} + Q_{nI} \tag{30}$$

Note that for node I representing the well the volumetric flux Q_{lI} and the mass flux $\dot{M}_{lI}$ are related by $\dot{M}_{lI} = \rho_l Q_{lI}$ ($l = w, n$). Within the effective flow area surrounding the node the flow of each phase is assumed to be in a quasi steady state, and the average fluid potential is Φ_{lI}. To facilitate an analytical solution of the local grid block well flow problem we introduce a concentric circle of radius r_e. The analytical solution domain is thus bounded by $r_B \le r \le r_e$. Formulas for determining r_e can be found in several references [*Peaceman*, 1983; *Pritchett and Garg*, 1980; *Abou-Kassem and Aziz*, 1985]. At the well boundary, $r = r_w$ and $\Phi_l = \Phi_{wB}$ (the potential of the fluid in the well bore). Using the radial flow analytical solution given by *Dake* [1978, p. 146], Q_{lI} may be expressed as

$$Q_{lI} = G_{BI}\lambda_{lI}(\Phi_{lI} - \Phi_{wB}) \tag{31}$$

where λ_{lI} is a mobility factor for phase l at node I, and G_{BI} is the well bore index. These coefficients are defined as

$$\lambda_{lI} = \bar{k}_{rlI}/\mu_l \tag{32a}$$

$$G_{BI} = \frac{2\pi\bar{k}b}{\ln(r_e/r_B) + S_F - f} \tag{32b}$$

where $\bar{k}_{rl}$ and $\bar{k}$ are the pseudowell relative and intrinsic permeabilities that are vertically averaged by integrating over the screen length of the well, instead of the liquid-saturated thickness. Here f is a constant equal to 0.5 for the quasi-steady flow solution, and S_F is a skin factor of the well and is usually set to zero. Substitution of (31) into (30) gives

$$\Phi_{wB} = \frac{-Q_L + \lambda_{nI}\Phi_{nI} + \lambda_{wI}\Phi_{wI}}{\lambda_{nI} + \lambda_{wI}} \tag{33}$$

physical constraint

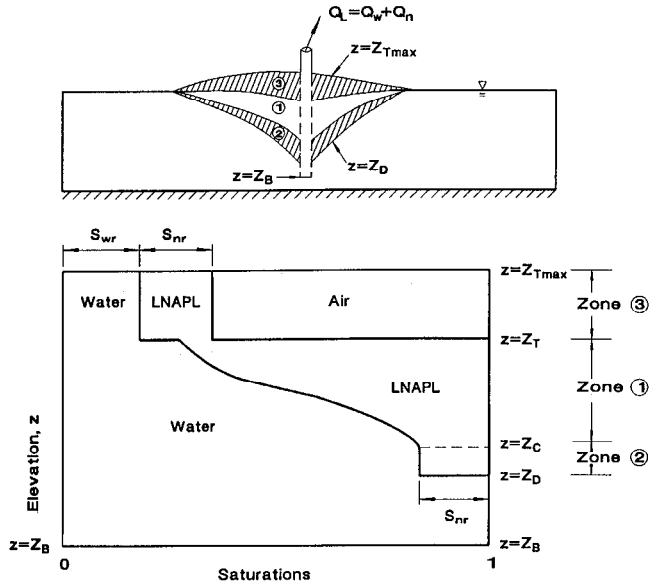

Figure 3. Groundwater remediation scenario and typical GCVE model prediction of LNAPL zones and saturation profiles.

$$\Phi_{wB} \ge \Phi_{\min} \tag{34}$$

where $\Phi_{\min}$ is a user-input minimum well bore potential value. If (34) is violated, the target rate, Q_L, cannot be achieved, the well is placed on deliverability with $\Phi_{wB} = \Phi_{\min}$, and the flow rate is still computed using (31). The model has the capability to switch from rate to potential constraints (or vice versa) in the course of simulation, as required in response to changes in aquifer pumping conditions.

In the situation when a bottom hole pressure or Φ_{wB} is specified, the valumetrical rates for water and NAPL are directly computed using (31).

In the treatment of either prescribed pumping rates or well bore potentials through production wells, mass fluxes of fluids are evaluated using the above formulation and added to the residual equation (27). The corresponding terms in the Jacobian are then modified accordingly.

Interpretation of Model Output

For a practical scenario involving LNAPL contamination in an unconfined aquifer and remediation by well pumping, three distinct LNAPL zones may be delineated, as shown in Figure 3. Zone 1 is the zone of mobile LNAPL, wherein $S_{nr} < S_n \le 1 - S_{wr}$, and the vertical profiles of water and LNAPL saturations follow the rock capillary pressure curve. This zone is bound by the current positions of the LNAPL table ($z = Z_T$) and the mobile LNAPL/water contact ($z = Z_c$). The other two zones (2 and 3) exist because of the effect of pumping. Zone 2 is the underlying zone of immobile LNAPL, wherein the LNAPL saturation is at the irreducible (residual) value. This zone is bound by the surfaces of $z = Z_C(x, y)$ and $z = Z_D(x, y)$. Note that Z_D is also history-dependent, as explained in the previous sections. Since the aquifer is unconfined, the free-surface position, which corresponds to the top liquid table, is also vation of the LNAPL table tracked by the model up to the

present time, then zone 3 is identified as the aerated zone bounded by the surfaces defined by $z = Z_{T\max}(x, y)$ and $z = Z_T(x, y)$. Within this zone both the LNAPL and the water phase are regarded as immobile (i.e., $S_n = S_{nr}$ and $S_w = S_{wr}$). Furthermore, capillary effects are neglected in the aerated zone via the use of free-surface boundary condition treatment. This leads to the discontinuities in the values of S_n and S_w at $z = Z_T$ (see Figure 3). As the pumping operation continues, zone 1 continues to shrink and eventually diminishes, leaving behind the residual LNAPL saturation in the remaining two zones.

In simulating areal flow in an unconfined aquifer the model also allows a simplified treatment of the top boundary ($z = Z_T$) of the flow domain. If the drawdown resulting from well pumping is relatively small (as compared to the liquid-saturated thickness), Z_T may be regarded as constant with time. Consequently, only zones 1 and 2 need to be delineated by the model. This is also the case if the aquifer system is confined.

Another simulation output that is desirable for assessing the effectiveness of a remedial design is the relationship between cumulative recovery of LNAPL (usually expressed in terms of pore volume) versus time since the start of pumping. The knowledge of the LNAPL recovery curve is also essential for a cost-benefit analysis of the remedial operation.

Verification and Simulation Examples

In this section, three examples are provided to demonstrate verification and utility of the GCVE model and to check numerical accuracy and validate the vertical equilibrium assumptions. Simulation results obtained using the GCVE modeling approach are compared with analytical solutions, laboratory experimental data, and rigorous multiphase numerical solutions that take into account vertical flow components.

Table 1. Data Used in the Simulation of Linear Displacement of Oil by Water

Parameter	Value
Reservoir thickness b	20 ft
Base elevation Z_B	0
Distance between injectors and producers L_x	1000 ft
Distance between injection wells L_y	300 ft
Rate of water injection for each injection well	338 RB d^{-1}
Porosity ϕ	0.15
Intrinsic permeability k	0.2 darcy
Water density ρ_w	62.4 lb ft^{-3}
Oil density ρ_n	49.92 lb ft^{-3}
Water viscosity μ_w	1 cP
Oil viscosity μ_n	2 cP
Residual water saturation S_{wr}	0.363
Residual oil saturation S_{nr}	0.205
Initial oil saturation $S_n(t = 0)$	0.637

Units are 1 ft = 3.048 m; 1 reservoir barrel (RB) = 5.614 ft^3 = 1.59 hL; 1 cP = 10^{-3} Pa s; 1 lb ft^{-3} = 16.02 kg m^{-3}.

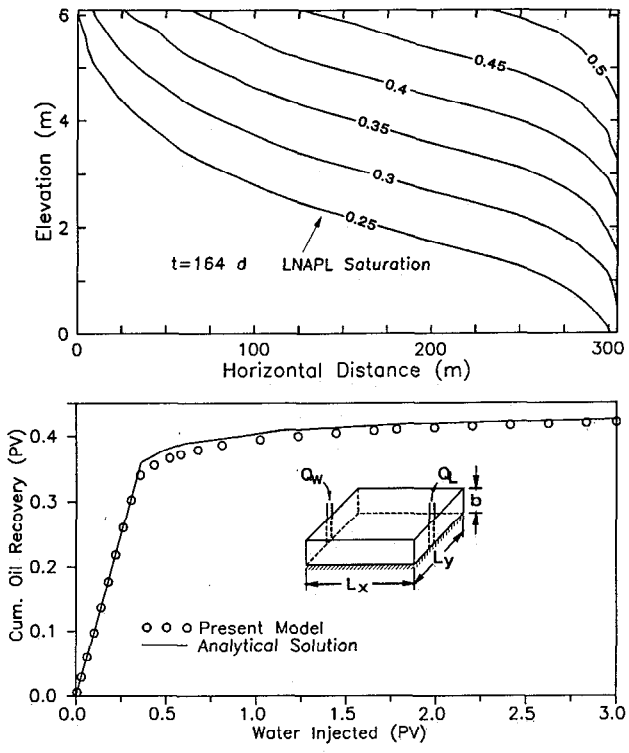

Figure 4. Predicted oil saturation and cumulative oil recovery volume resulting from a linear waterflood displacement.

Linear Displacement of Oil by Water

In this example we consider a well-known reservoir engineering problem involving linear displacement (direct line drive) of oil by water in a homogeneous formation under vertical equilibrium of capillary and gravitational forces. The analytical solution to the problem was computed by *Willhite* [1986, Figure 5.16] based on the GCVE concept.

The physical parameter values used in our simulation are listed in Table 1. The rock capillary and relative permeability data are the same as used by *Willhite* [1986]. Note that the rectangular domain of the GCVE numerical model is of dimensions L_x = 1000 ft (304.5 m) and L_y = 300 ft (91.4 m) along the x and y axes, respectively. The reservoir thickness is 20 ft (6.1 m). At $x = 0$ the boundary condition for each injection well: Q_w = 338 RB d^{-1} (1 reservoir barrel (RB) = 5.614 ft^3 (1.59 hL)) was imposed. At x = 1000 ft (304.8 m) the production rate boundary condition (Q_L = 338 RB d^{-1}) for each pumping well was imposed. The domain was discretized using a uniform rectangular grid consisting of 50 elements and 102 nodes (52 columns and 2 rows). The oil saturation distribution and cumulative oil recovery as a function of pore volume of water injected are plotted in Figure 4 together with the schematic description of the problem. The numerical result of cumulative oil recovery is in very good agreement with the analytical curve given by *Willhite* [1986]. Notably, the numerical model slightly underpredicts the cumulative oil recovery volume.

Migration of LNAPL in a Cross Section of Unconfined Aquifer

This example is selected to verify and demonstrate application of the GCVE modeling approach to a typical LNAPL

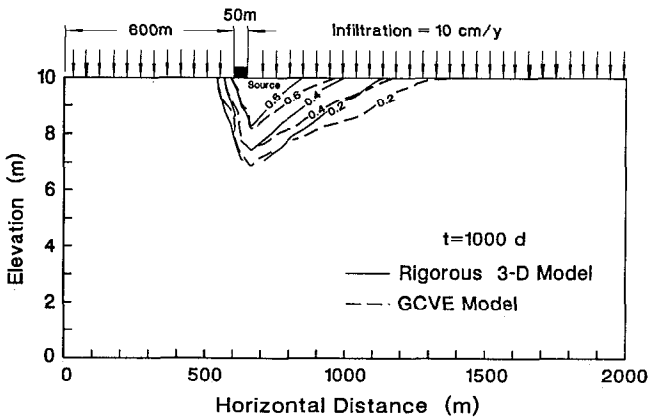

Figure 5. LNAPL saturation contour predicted by the GCVE and the rigorous three-dimensional multiphase models.

contamination scenario. The problem concerns an unconfined aquifer that is contaminated by a continuous release of organic chemical at a rate of 1000 kg yr^{-1} m^{-2} from a 50-m-long source, as illustrated in Figure 5. The aquifer is subject to steady infiltration at a rate of 10 cm yr^{-1}. Ambient groundwater flow is assumed to occur with a hydraulic gradient of 1.41%. The aquifer properties are as follows: k = 6.4 × 10^{-2} m^2, ϕ = 0.3, and S_{wr} = S_{nr} = 0.2. Groundwater properties are ρ_w = 1000 kg m^{-3} and μ_w = 1 cP (10^{-3} Pa s). LNAPL properties are ρ_n = 900 kg m^{-3} and μ_n = 0.64 cP (10^{-3} Pa s). The relative permeability and capillary pressure data is given in Table 2.

The problem was analyzed using both the GCVE simulator and rigorous multiphase simulator [*Huyakorn et al.*, 1992a], which accounts for both horizontal and vertical flow components. The grid used for discretizing the cross-sectional domain of the multiphase model has grid line coordinates of 0, 56, 256, 427, 533, 600, 612, 625, 638, 650, 717, 817, 967, 1167, 1367, 1567, 1767, 1967, and 2000 m in the x direction, and 0, 1, 2, 3, 4, 4.5, 5, 5.5, 6, 6.5, 7, 7.5, 8, 8.5, 9, 9.5, and 10 m in the vertical (z) direction. The grid used for the GCVE model is the same in the x direction as the grid of the multiphase model, the vertical dimension being reduced via the integration using the VE concept. The CPU time requirement for the areal GCVE simulation was approximately 10 min on PC386/25 MHz and was an order of magnitude less than the fully three-dimensional multiphase simulation. Saturation distributions of LNAPL after 1000 days of release from the source are shown in Figure 5 for both simulation approaches.

As can be seen, the predictions given by the two models are in good agreement. Note that the lowest saturation contour given by the GCVE model is 0.2, which corresponds to the residual saturation. For the three-dimensional model the 0.1 saturation contour was produced by linear interpolation of the numerical values which vary from 0.2 to nearly zero between two adjacent grid points. A further illustration of the close agreement between the GCVE and fully three-dimensional modeling results is presented in Figure 6, where saturation profiles along the vertical center beneath the contaminant source are plotted for two time values.

Table 2. Relative Permeability and Capillary Pressure Data Used in the Simulation of LNAPL Migration in a Cross Section

S_w	k_{rw}	k_{rn}	p_c, Pa
0.200	0.000	0.680	0.9000E+04
0.300	0.040	0.550	0.5400E+04
0.400	0.100	0.430	0.3900E+04
0.500	0.180	0.310	0.3300E+04
0.600	0.300	0.200	0.3000E+04
0.700	0.440	0.120	0.2700E+04
0.800	0.600	0.000	0.2400E+04
0.900	0.800	0.000	0.1500E+04
1.000	1.000	0.000	0.0000E+00

Read 0.9000E+04 as 0.9000 × 10^4.

Waterflood Behavior of Laboratory Five-Spot Well Pattern

This example concerns the model validation using laboratory experimental data for oil recovery from a five-spot well pattern. The cumulative oil recovery curves obtained from several laboratory waterfloods were presented by *Gaucher and Lindley* [1960]. One of the waterflood tests was simulated by *Coats et al.* [1967] using their areal GCVE and fully three-dimensional numerical models. The selected waterflood was scaled to represent a production rate of 42 RB d^{-1} (1 reservoir barrel (RB) = 5.614 ft^3 (1.59 hL)) into a 20-acre (8.1 ha), five-spot system reservoir having intrinsic permeability of 16 mdarcy and thickness of 20 ft (6.1 m) (see Figure 7). Hydraulic properties reported by Gaucher and Lindley for the fluids and unconsolidated sand were used by *Coats et al.* [1967] in their simulations. However, these authors did not report the capillary pressure and relative permeability data used to obtain their modeling results.

For model validation purposes we selected the same case previously simulated by *Coats et al.* [1967]. The data required by the GCVE model are summarized in Table 3. Note that the tabulated values of capillary pressure and relative permeabilities were determined using the functional expressions given by *Willhite* [1986, pp. 71, 150] and direct substitution of the known hydraulic parameter values k, S_{wr}, S_{nr}, k^*_{rw}, and k^*_{rn}. The exponents and coefficients of the relative permeability functions used were treated as the undetermined parameters to apply the given values of k^*_{rw} and k^*_{rn}.

A square diagonal grid (467 ft × 467 ft) (142.3 m) covering an area of 5 acres (2 ha) was adopted for the numerical

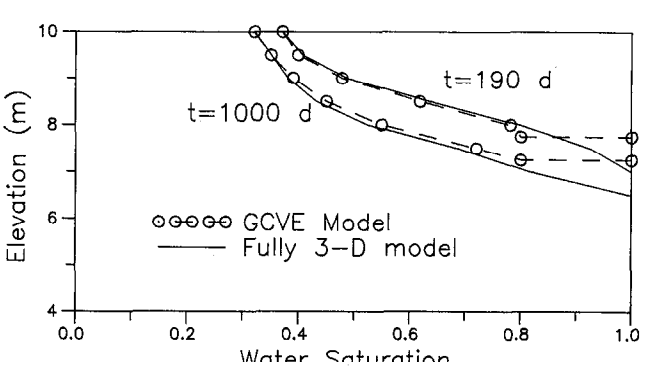

Figure 6. Vertical distributions of LNAPL saturation beneath the contaminant source.

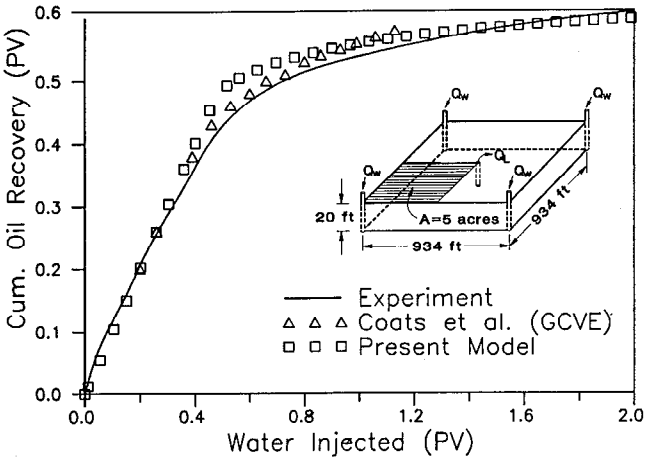

Figure 7. Experimental and simulated behavior of laboratory five-spot waterflood.

solution. The grid spacings were $\Delta x = \Delta y = 46.7$ ft (14.2 m). The experimental data and simulation results obtained from the present and previous models are compared in Figure 7. Note that the areal GCVE and three-dimensional simulation results given by *Coats et al.* [1967] are in excellent agreement. The present GCVE model predicts slightly higher oil recovery over the range of 0.3 to 0.8 pore volumes of water injection. Much of the discrepancy may be attributed to the difference in the soil functions used in the present and previous simulations.

Mass Balance Results

The mass balance data for the three simulation samples are provided in Table 4. As can be seen from the table, the mass balance errors of the present model are almost zeros for all the cases. This is true for all the simulations we have done with the GCVE model. The mass-conservative numerical scheme, such as implemented in the present model, will guarantee good mass balance results regardless of time step size or spatial discretization, as long as a converged solution is obtained.

Table 3a. Data Used in the Reservoir-Scale Simulation of a Waterflood Five-Spot Laboratory Experiment Reported by *Gaucher and Lindley* [1960]

Parameter	Value
Water injection rate Q_w	42 RB d^{-1} per well
Total liquid production rate Q_L	42 RB d^{-1} per well
Intrinsic permeability k	16 mdarcy
Porosity ϕ	0.2
Oil density ρ_n	49.92 lb ft^{-3}
Oil viscosity μ_n	2.17 cP
Water density ρ_w	62.4 lb ft^{-3}
Water viscosity μ_w	0.5 cP
Residual water saturation S_{wr}	0.3
Residual oil saturation S_{nr}	0.067
Water relative permeability at residual oil saturation k^*_{rw}	0.562
Oil relative permeability at residual water saturaion k^*_{rn}	0.813
Initial oil saturation $Sn(t = 0)$	0.7

Units are 1 lb ft^{-3} = 16.02 kg m^{-3}; 1 cP = 10^{-3} Pa s.

Table 3b. Soil Functions for the Reservoir-Scale Simulation of a Waterflood Five-Spot Laboratory Experiment Reported by *Gaucher and Lindley* [1960]

S_w	k_{rw}	k_{rn}	p_c, Pa
0.30000	0.00000	0.81250	0.4434*E*+05
0.33164	0.00000	0.75002	0.3810*E*+05
0.36328	0.00000	0.68935	0.3295E+05
0.39492	0.00000	0.63055	0.2863*E*+05
0.42656	0.00000	0.57365	0.2495*E*+05
0.45820	0.00001	0.51870	0.2177*E*+05
0.48984	0.00005	0.46578	0.1901*E*+05
0.52148	0.00016	0.41492	0.1658*E*+05
0.55312	0.00046	0.36622	0.1443*E*+05
0.58476	0.00115	0.31973	0.1251*E*+05
0.61640	0.00261	0.27556	0.1079*E*+05
0.64804	0.00547	0.23379	0.9237*E*+04
0.67968	0.01073	0.19455	0.7828*E*+04
0.71132	0.01996	0.15797	0.6545*E*+04
0.74296	0.03545	0.12420	0.5371*E*+04
0.77460	0.06051	0.09346	0.4293*E*+04
0.80624	0.09979	0.06598	0.3300*E*+04
0.83788	0.15963	0.04212	0.2381*E*+04
0.86952	0.24860	0.02238	0.1530*E*+04
0.90116	0.37799	0.00759	0.7380*E*+03
0.93280	0.56250	0.00000	0.0000*E*+00

Read 0.4434*E*+05 as 0.4434×10^5.

Conclusions

The areal numerical model presented herein was developed to simulate the simultaneous flow of groundwater and a nonaqueous phase liquid (NAPL) for specific application to petroleum or chemical spills and leaks and remedial design and evaluation. The gravity-capillary vertical equilibrium (GCVE) formulation described incorporates history-dependent pseudo capillary and relative permeability functions. These functions were developed to allow realistic simulations of migration and remediation scenarios involving partly contaminated groundwater systems and significant residual NAPL saturations. Although attention was specifically focused on LNAPL, the formulation could be readily adapted to denser NAPL (DNAPL). Pumping wells with prescribed total production rates and bottom hole pressures were treated in a rigorous manner using fully implicit schemes that incorporate the effects of well radius.

Robust and efficient mass-conservative numerical solution techniques were implemented to allow complete analyses of site-specific field problems on personal computers or workstations. Simulation examples were provided to demonstrate the model verification and utility. Both analytical and rigorous multiphase (cross-sectional and three-dimensional) numerical solutions were used to check the results from the GCVE formulation. For the various test cases the GCVE performed remarkably well, yielding good accuracy in predicting of vertical profiles of NAPL saturation and cumulative recovery curves. When validated against a laboratory experiment on waterfloods in a five-spot reservoir, the [illegible] ing the free-product recovery curve that was in good agree-

Table 4. Mass Balance Results From the Three Simulation Examples

Example	Simulation Time, years	Mass Balance Error,* %	
		NAPL	Water
Linear displacement	1.9	1.8×10^{-3}	1.3×10^{-3}
Migration in a cross section	3.0	1.5×10^{-2}	1.0×10^{-3}
Five-spot waterflood	94.0	2.6×10^{-6}	1.6×10^{-2}

*Mass balance error is defined as mass balance error = cumulative mass storage increase − cumulative net outflow × 100 (|cumulative mass storage increase|)$^{-1}$.

ment with the experimental data and previous model predictions. The comparative study reported here indicates the validity of the vertical equilibrium (VE) assumptions for practical scenarios concerning the contamination and remediation of groundwater systems. In performing a realistic field simulation the CPU time required by the GCVE modeling approach was generally less than 10% of that required by the fully three-dimensional multiphase modeling approach. The contrast in CPU requirements would be even more drastic in situations involving more highly nonlinear capillary pressure and relative permeability curves of the soil or rock material. This is because the pseudo functions are generally less nonlinear than the real soil functions.

References

Abou-Kassem, J. H., and K. Aziz, Analytical well models for reservoir simulation, *Soc. Pet. Eng. J.*, *25*, 573–579, 1985.

Abriola, L. M., and G. F. Pinder, A multiphase approach to the modeling of porous media contamination by organic compounds, 2, Numerical simulation, *Water Resour. Res.*, *21*, 19–26, 1985.

Coats, K. H., R. L. Nielsen, M. H. Terhune, and A. G. Weber, Simulation of three-dimensional, two-phase flow in oil and gas reservoirs, *Soc. Pet. Eng. J.*, *7*, 377–388, 1967.

Coats, K. H., J. R. Demsey, and J. H. Henderson, The use of vertical equilibrium in two-dimensional simulation of three-dimensional reservoir performance, *Soc. Pet. Eng. J.*, *11*, 63–71, 1971.

Dake, L. P., *Fundamentals of Reservoir Engineering*, Elsevier, New York, 1978.

Faust, C. R., Transport of immiscible fluids within and below the unsaturated zone: A numerical model, *Water Resour. Res.*, *21*(4), 587–596, 1985.

Faust, C. R., J. H. Guswa, and J. W. Mercer, Simulation of three-dimensional flow of immiscible fluids within and below the unsaturated zone, *Water Resour. Res.*, *25*, 2449–2464, 1989.

Forsyth, P. A., Simulation of nonaqueous phase groundwater contamination, *Adv. Water Resour.*, *11*, 74–83, 1988.

Forsyth, P. A., A control volume finite element approach to NAPL groundwater contamination, *Soc. Ind. Appl. Math J. Sci. Comput.*, *12*(5), 1029–1057, 1991.

Gaucher, D. H., and D. C. Lindley, Waterflood performance in a stratified, five-spot reservoir, a scaled-model study, *Trans. Am. Inst. Min. Metall. Pet. Eng.*, *219*, 208–215, 1960.

Hochmuth, D. P., and D. K. Sunada, Ground-water model of two-phase immiscible flow in coarse material, *Ground Water*, *23*(5), 617–626, 1985.

Huyakorn, P. S., Y. S. Wu, S. Panday, and N. S. Park, MAGNAS3: Multiphase analysis of groundwater, non-aqueous phase liquid and soluble component, version 1.0, code documentation report, HydroGeoLogic, Incorporated, Nov. 1992a.

Huyakorn, P. S., Y. S. Wu, and S. Panday, A comprehensive three-dimensional numerical model for predicting the transport and fate of petroleum hydrocarbons in the subsurface, paper presented at Petroleum Hydrocarbons and Organic Chemicals in Ground Water: Prevention, Detection, and Restoration, Natl. Ground Water Assoc., Houston, Tex., Nov. 4–6, 1992b.

Kaluarachchi, J. J., and J. C. Parker, An efficient finite element method for modeling multiphase flow, *Water Resour. Res.*, *25*, 43–44, 1989.

Kaluarachchi, K., J. C. Parker, and R. J. Lenhard, A numerical model for areal migration of water and light hydrocarbon in unconfined aquifers, *Adv. Water Resour.*, *13*(1), 29–40, 1990.

Letniowski, F., and P. A. Forsyth, A control volume finite element method for three-dimensional NAPL contamination, *Int. J. Numer. Methods Fluids*, *13*, 955–970, 1991.

Martin, J. C., Partial integration of equations of multiphase flow, *Pet. Eng. J.*, *8*, 370–380, 1968.

Parker, J. C., and R. J. Lenhard, Vertical integration of three-phase flow equations for analysis of light hydrocarbon plume movement, *Transp. Porous Media*, *5*, 187–206, 1989.

Parker, J. C., J. J. Kaluarachchi, V. J. Kremesec, and E. L. Hockman, Modeling free product recovery at hydrocarbon spill sites, paper presented at Petroleum Hydrocarbons and Organic Chemicals in Ground Water: Prevention, Detection, and Restoration, Natl. Water Well Assoc., Houston, Tex., Oct. 31–Nov. 2, 1990.

Parker, J. C., J. Zhu, and H. White, Modeling phase separated hydrocarbon migration and recovery in anisotropic fractured media, paper presented at Petroleum Hydrocarbons and Organic Chemicals in Ground Water: Prevention, Detection, and Restoration, Natl. Water Well Assoc., Houston, Tex., Nov. 4–6, 1992.

Peaceman, D. W., Interpretation of well block pressures in numerical reservoir simulation with nonsquare grid blocks and anisotropic permeability, *Soc. Pet. Eng. J.*, *13*, 531–543, 1983.

Pritchett, J. W., and S. K. Garg, Determination of effective well block radii for numerical reservoir simulations, *Water Resour. Res.*, *16*(4), 665–674, 1980.

Willhite, G. P., Waterflooding, in *Society of Petroleum Engineering*, Textbook, vol. 3, 326 pp., Society of Petroleum Engineering, New York, 1986.

P. S. Huyakorn, N. S. Park, and Y. S. Wu, HydroGeoLogic, Incorporated, 1165 Herndon Parkway, Suite 900, Herndon, VA 22070.

(Received September 8, 1993; revised September 9, 1993; accepted November 30, 1993.)